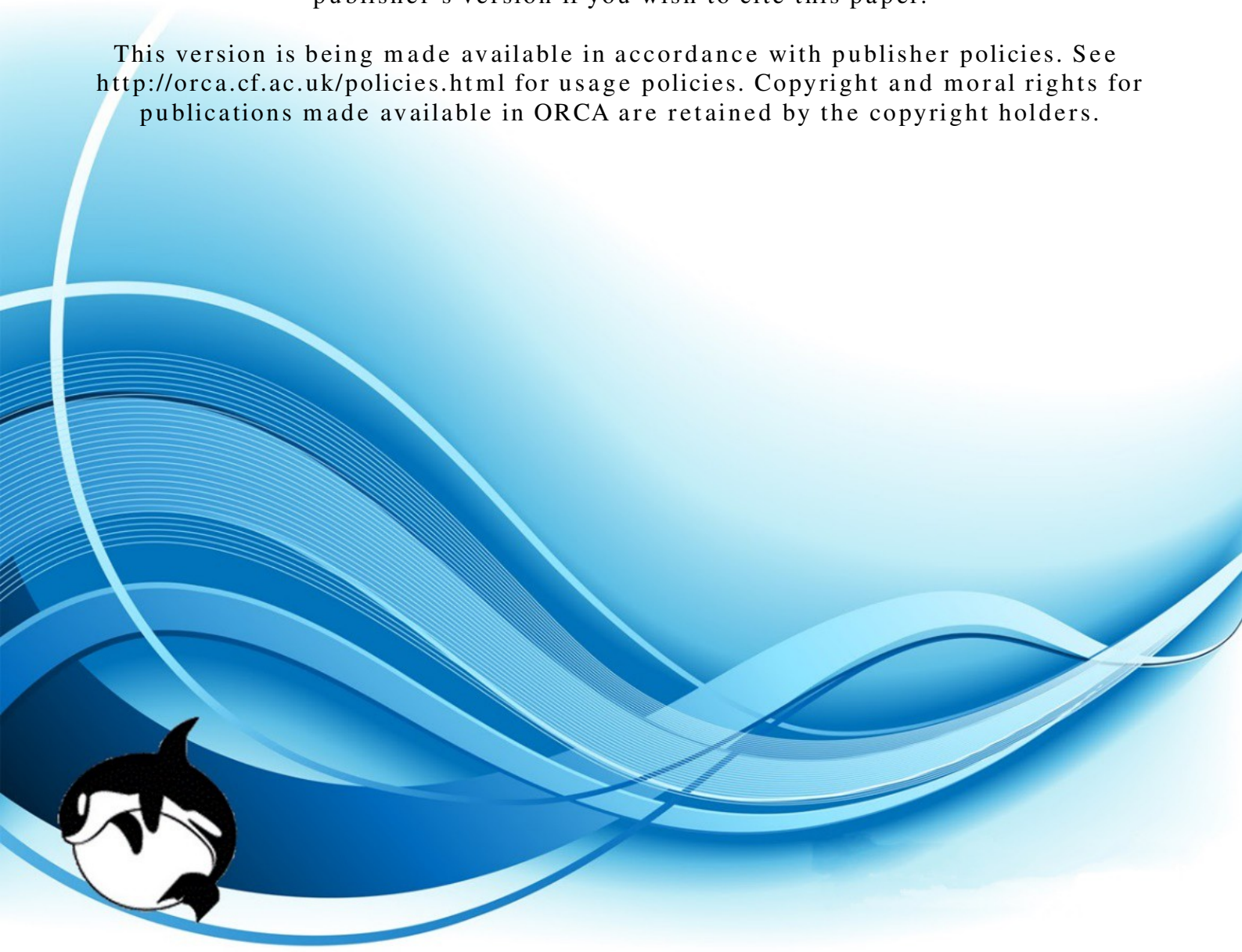

Theoretical Study of Copper binding to GHK peptide

Nadiyah Alshammari and James A. Platts*

School of Chemistry, Cardiff University, Park Place, Cardiff CF10 3AT, UK

* Author for correspondence: platts@cardiff.ac.uk +44-2920-874950

Abstract

We report ligand field molecular mechanics, density functional theory and semi-empirical studies on the binding of Cu(II) to GlyHisLys (GHK) peptide. Following exhaustive conformational searching using molecular mechanics, we show that relative energy and geometry of conformations are in good agreement between GFN*2*-xTB semi-empirical and B3LYP-D DFT levels. Conventional molecular dynamics simulation of Cu-GHK shows the stability of the copper-peptide binding over 100ps trajectory. Four equatorial bonds in 3N1O coordination remain stable throughout simulation, while a fifth in apical position from C-terminal carboxylate is more fluxional. We also show that the automated conformer and rotamer search algorithm CREST is able to correctly predict the metal binding position from a starting point consisting of separated peptide, copper and water.

Introduction

GHK is a tripeptide consisting of glycine, histidine, and lysine (Gly-His-Lys) amino acids (Figure 1). Found naturally in blood plasma, urine and saliva[1], it was first isolated by Pickart et al in 1973 and identified as a liver cellular growth factor.[2] GHK has high binding affinity for copper and zinc cations, forming complexes whose function is believed to be mainly transport of Cu to cells[3]. After the Cu-GHK complex was identified, it has been investigated in numerous *in vivo* and *in vitro* studies, which indicate its wide range of biological functions. The exchange dynamics and redox behavior of GHK-Cu are stable in biological system as reported experimentally,[4] which makes it safe towards lipids and amino acids when copper is being transported to the cells[5–7].

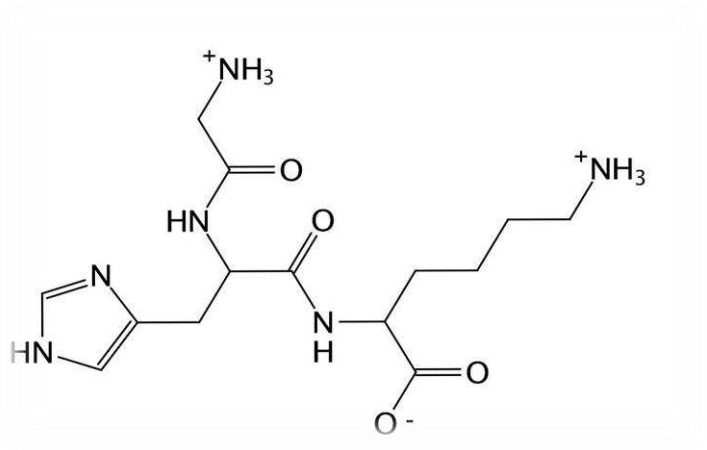

Figure 1: GHK structure

The Cu-GHK complex plays significant positive roles in the body, promoting wound healing, acting as an anti-inflammatory agent, and promoting cell growth and stimulating skin cell regeneration[8,9]. It also has been established that Cu-GHK has potential as an anticancer agent, and that it can repair damaged cells by accelerating DNA replication for cancer patients after radiation therapy[10]. It also shows potency toward neurodegenerative diseases such as Alzheimer's and Prion disease by protecting neurons from amyloid-β(Aβ) aggregation through competitive chelation to copper instead, which in turn decreases neurotoxicity[11].

The well-documented chemical and physiological activity of Cu-GHK makes it interesting in its own right, while its relatively small size makes is a useful model for binding of metal ions to larger peptides. Hence, the structural and coordinating properties of Cu-GHK complex have been given much attention in recent years. Several experimental studies have probed the structure and behaviour of Cu-GHK in different conditions, including X-ray crystallography,

NMR, EPR, IR, electronic absorption and Raman spectroscopy, as well as calorimetry and titration[4,6,12–14]. The structure obtained from X-ray studies shows the complex forms when Cu (II) chelates to the histidine side chain, glycine-α amino group and deprotonated nitrogen from the glycine-histidine peptide bond. Perkins et al[6] reported Cu-GHK crystal structure in which three different peptides link one Cu ion through 3N2O coordination; three nitrogen atoms come from one peptide, while the other oxygens come from two separate peptides. Hureau at el[15] reported a binuclear structure, with two copper atoms in solid state, resulting in penta-coordinated, distorted square pyramid around Cu, with 3N1O in equatorial positions and a further oxygen occupying the apical position, in which Cu binds to three N-atoms from the same GHK, while two O atoms come from lysine of neighbouring tripeptide.

In contrast, in solution the complex forms a mononuclear structure, indicating rupture of dimeric structure that is present in solid state. Hence, it is possible that the equatorial oxygen position, provided by carboxylate group of neighbouring lysine in the crystal, is displaced by solvent molecule in liquid state. The source of this fourth oxygen-copper bond is provided from water (solvent) or carboxyl groups of lysine from neighbouring GHK[5–7,15]. All studies indicate distorted square pyramidal geometry around Cu, in which four ligands are equatorial with distance about 2.0 Å, with the remaining apical ligand slightly farther from copper at around 2.5 Å.

Hureau et al also studied reactive oxygen species (ROS) production from Cu-GHK peptide using cyclic voltammetry, fluorescence, and EPR measurements[15]. This showed the difficulty for the complex to be reduced by ascorbate, indicating redox silencing of Cu(II) when bound to GHK peptide. However, another study by Guilloreau et al[16] suggested that Cu-GHK catalyses formation of reactive species such as the hydroxyl radical, HO·.

Even with all this experimental data, there are challenges to determining the structure and conformation of Cu-GHK due to flexibility and multiple potential metal binding sites. Electronic structure calculations can provide complementary information to experiments, and are an effective means for analysis of compounds containing transition metal ions,[17]and metal-biomolecule interactions[18]. However, modelling flexible peptides when bound to metal ions is challenging. Accurate quantum mechanical methods are computationally expensive, even for those methods that are relatively efficient such as density functional theory (DFT). Molecular mechanics (MM) is applicable for many problems in biochemistry for exploring

conformational space[19–24], but is not well suited for treatment of d-orbital effects in transition metals[25–28].

Combined QM/MM is effective for modelling metals in biomolecules[29–37], but the inclusion of QM methods can still compromise the computing expense. Therefore, alternative methods that reduce computational time with reliable accuracy are attractive. Ligand field molecular mechanics (LFMM) was introduced by Deeth and co-workers, including explicit d-electron energy terms for transition metals to the standard MM expression[38,39]. This has previously been used to study small[40,41] and large metal-biomolecular systems such as metalloproteins[42,43], including a range of transition metals such as Cu and Pt[44–49]. Recently, our group showed that LFMM is suitable for predicting geometries and exploring the conformational space of transition-metals such as Cu(II) and Pt(II) when bound to amyloid-β peptide, although we found this method fails to reproduce DFT energy[44].

Semiempirical methods recently developed by Grimme, termed GFN2-xTB,[50,51] have been proposed for calculating molecular geometries, vibrational frequencies, and non-covalent interaction energies. They have been shown to sample geometries in much shorter time than DFT with high accuracy, are applicable to heavy elements up to radon (Z=86), and are tested in literature on large metal-complex system[52–55]. This high performance makes it potentially suitable for our systems of interest, *i.e.* metal-peptide complexes.

In this work, we test LFMM and GFN2-xTB approaches for describing metal coordination to GHK, using DFT methods as a benchmark, then apply these to examine the dynamical behaviour of GHK-Cu using molecular dynamics (MD).

Computational Method

The Cu(II)-GHK system was set up in MOE as follows. The sequence, Gly-His-Lys was constructed in extended geometry with all peptide bonds in *trans*- orientation. Cu(II) was coordinated to the neutral N-terminus of Gly, deprotonated N of Gly-His peptide bond, and either Nε/Nδ of the His imidazole ring, and to O of a single water molecule in equatorial position to form distorted square planar geometry, as reported by Hureau and co-workers[15]. The overall charge on the complex is +1, arising from +2 on Cu and +1 from protonated Lys balanced against deprotonated peptide N and carboxylate C-terminus. Low mode MD and stochastic [56,57] conformational exploring were organized through MOE, using LFMM for Cu

and coordinated atoms, and AMBER94[58] force parameter for the remainder of the peptide. Parameters for Cu-N_{his} and Cu-N_{amine} were reported previously,[59] while parameters for Cu—OH_2 and Cu—N_{pept} were estimated by analogy with chemically similar species, the former using peptide backbone O as a guide, the latter using N_{His}. Ligand field molecular mechanics (LFMM)[39] calculations were carried out by the DommiMOE extension to the Molecular Operating Environment (MOE)[60]. Two distinct conformational searching methods were used to provide more data for benchmarking: both include geometry optimisation, such that all MM geometries and energies are, by definition, are at local minima.

Conformers generated from LFMM were used for DFT single-point calculations and geometry optimization. B3LYP-D2[10,11] with def2-SVP[12, 13] basis set was extensively used, since this was also used as a benchmark in previous work,[59] though for comparison we also examined the performance of B3LYP-D3, PBE[65,66], PBE0[67,68] also with D3[69] as well as M06-2x[70] and ωB97xD[71]. DFT calculations used the polarizable continuum model (PCM) and the conductor-like polarizable continuum model (CPCM). Geometry optimization using semiempirical GFN2-xTB methods employed a generalized Born-surface area (GB-SA) model of aqueous solvent. DFT calculations were performed using Gaussian09[72] and ORCA[73] software. Semi-empirical calculations were performed via the XTB program[74]. Visual molecular dynamics (VMD)[75] program was used for trajectory analysis.

Further conformational searches were done by conformer-rotamer ensemble sampling tool (CREST)[53,76] approach, within the xtb suite of programs, that conjugates metadynamics sampling (MTD), and genetic z-matrix crossing (GC)[77]. Molecular dynamics simulations were performed using xtb within the NVT ensemble with timestep of 4.0 fs, facilitated by all bond lengths being restrained using the SHAKE algorithm and fictitious hydrogen mass of 4 amu, at 310 K.

Result and discussion

The result of conformational search shows that while coordination of Nε and Nδ of His imidazole ring to Cu are both possible, Nδ is markedly more favorable, resulting in an approximate square pyramidal geometry, and lower energy values by (-640 kJ mol^{-1} from LFMM/AMBER estimation) compared to Nε. The latter gives unfavorable 7-membered metallocycles, leading to the imidazole N-donor being located in axial position to copper, shown in figure 2, leading us to choose Nδ binding for subsequent calculations.

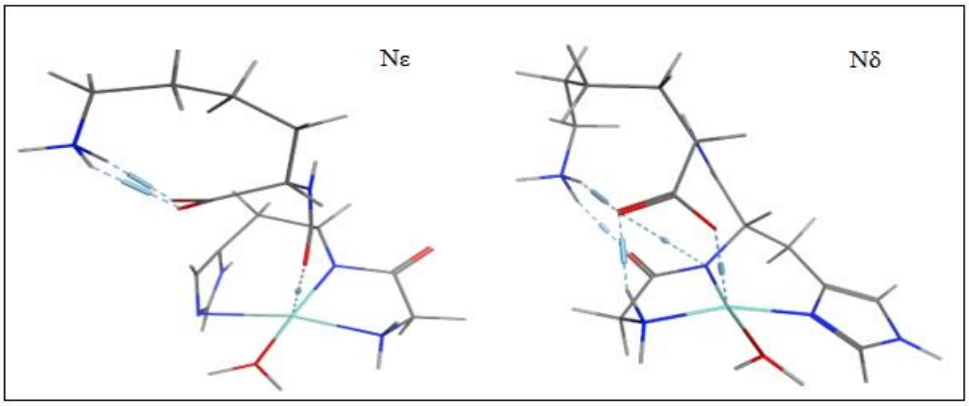

Figure 2:Nδ and Nε geometries

Low mode search finished with only three conformers, as shown in figure 3: each of these had *cis*- orientation of peptide, indicating that this changes during the conformational search. Superposition of conformations indicates that metal coordination remains constant, and flexibility is only found in the side-chain of Lys. For two conformations, the peptide was manually changed back to *trans*- and LFMMM optimised, but for the third conformer the rotation could not be achieved due to constraints of metal coordination, leading to a total of five conformers, named as cis1, cis2, cis3, trans1, and trans3. This small number of conformations generated from low mode search is due to limited flexibility of such a small peptide linked to copper. Applying the same search for the copper-free GHK peptide produced 118 conformers, clearly demonstrating the reduction in conformational flexibility on copper binding. Stochastic conformational search found 7 conformers of Cu-GHK with mutual RMSD of at least 0.5 Å, all with *trans*- orientation of peptides.

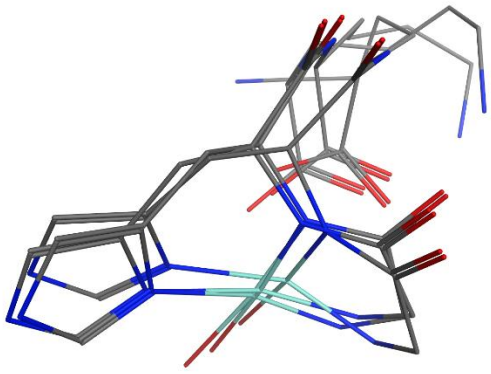

Figure 3: three cis-GHK low mode conformers

Despite the accuracy of DFT calculations, this method needs large computational expense for molecules of the size of metal-tripeptide. We therefore sought faster methods with acceptable accuracy for this system, and identified the, semi-empirical GFN*2*-xTB as a likely candidate for study of GHK-Cu complexes. However, it is important to test the results it provides. So, B3LYP-D2 and GFN*2*-xTB single point calculation was applied to the five conformer geometries obtained from Low Mode search, and relative energies compared. The resulting energies show correlation (R^2=0.73). After geometry optimization, the correlation between DFT and GFN*2*-xTB relative energy becomes stronger (R^2=0.89), as shown in Figure 4, despite taking no more than 2 minutes per conformation for GFN2-xTB. Also, GFN*2*-xTB and DFT exhibit similar trends as we move through the conformers labelled 1, 2, 3, 4 and 5 which corresponding to cis1,cis2, cis3,trans1,and trans3 using B3LYP-D2 optimised geometries, including multiple functionals, *i.e.* B3LYP-D3, PBE, PBE0, M06-2x and ωB97xD. The result shows those functionals are in general agreement with B3LYP-D2 and GFN*2*-xTB energy, as shown in figure 5. We also note that D2 and D3 dispersion corrections are in good agreement here, presumably due to the relatively small size of the Cu-GHK system.

In addition, GFN2-xTB geometries are in good agreement with those obtained from DFT geometry optimisation. RMSD values between GFN2-XTB and DFT optimised geometry are in the range 0.3 to 1.1 Å (cis1, 2, 3 = 0.31, 0.35, 0.49 Å; trans1 and 3 = 1.06, 0.70 Å). Furthermore, DFT/B3LYP-D2 single point calculation performed on seven conformers obtained from stochastic search at GFN*2*-xTB optimized geometry show good agreement between relative energies (R^2=0.64). Therefore, we conclude that GFN*2*-xTB reproduces DFT energies and geometries, but with much reduced calculation time.

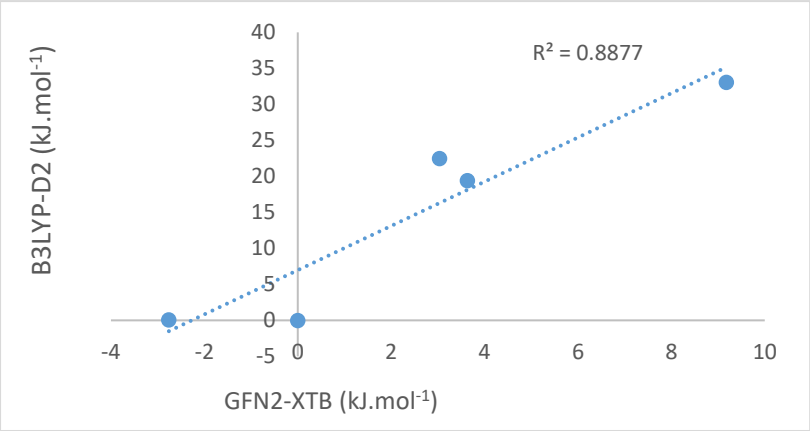

Figure 4: Relative energy of low mode conformers from B3LYP-D2 and GFN2-xTB

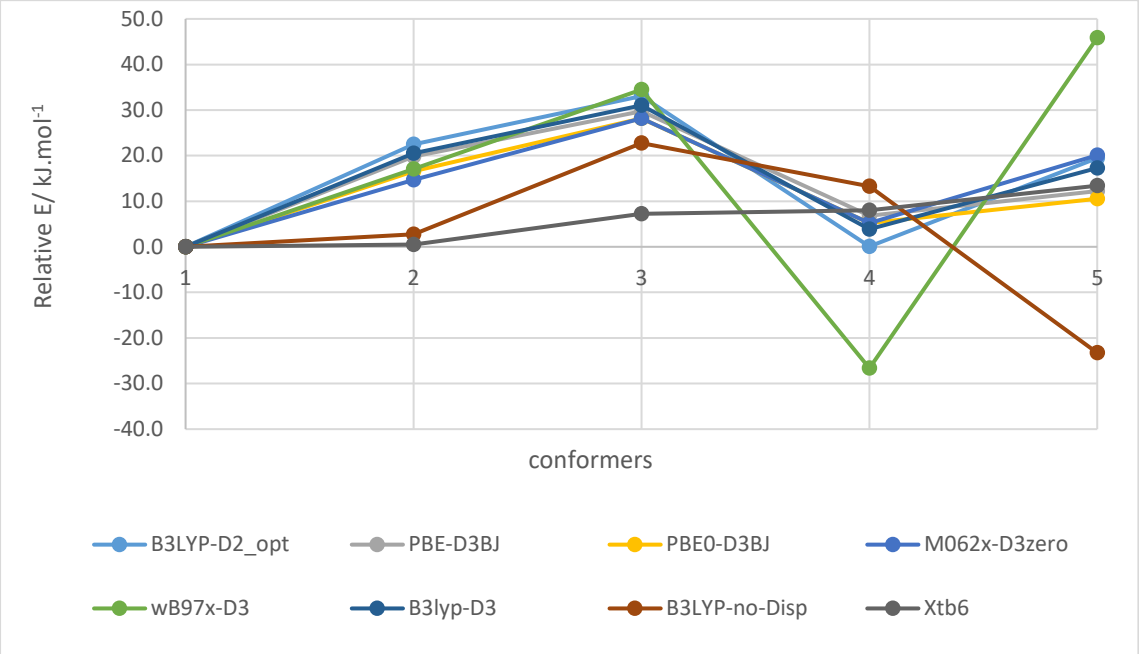

Figure 5: Relative energy for low mode conformers obtained by different methods as single point energy calculations at B3LYP-D2 optimised geometry. 1, 2, 3, 4 and 5 correspond to cis1,cis2, cis3,trans1,and trans3.

It is notable that most methods considered predict the cis1 conformation to have lowest energy. Closer inspection shows that cis1 has three hydrogen bonds compared to just two for trans1. For cis1, $-NH_3^+$ of Lys side chain interacts with peptide carbonyl from the same amino acid carboxylate and also to C-terminal carboxylate, while the third hydrogen bond forms between N-terminal $-NH_2$ of Gly and Lys carboxylate group. In trans1, the same interactions to carboxylate are present but the interaction with peptide carbonyl is lost (Figure S1, which may be origin of the stability of the *cis*- form.

The speed and accuracy of the GFN2-XTB method lends itself to dynamical simulations, so we first carried out conventional MD simulations at 310 K from low energy cis1 and trans1 conformations using GFN2-xTB. RMSD relative to starting point over a 100 ps trajectory is shown in Figure 6. Energy and temperature conservation over this timescale is shown in Supporting Information (Figure S4). This shows these geometries are stable over the simulation

timescale, typically remaining around 0.3 Å, although occasional increases to *ca.* 1 Å are observed in each case. Closer inspection shows that these increases do not involve the Cu-coordination sphere, but rather are due to changes in the orientation of the Lys side chain only. Table 1 shows the small average RMSD values and standard deviation for both trajectories. For comparison, equivalent MD simulations of the metal-free peptide were also performed (plot not shown), which show very similar RMSD statistics over this timescale.

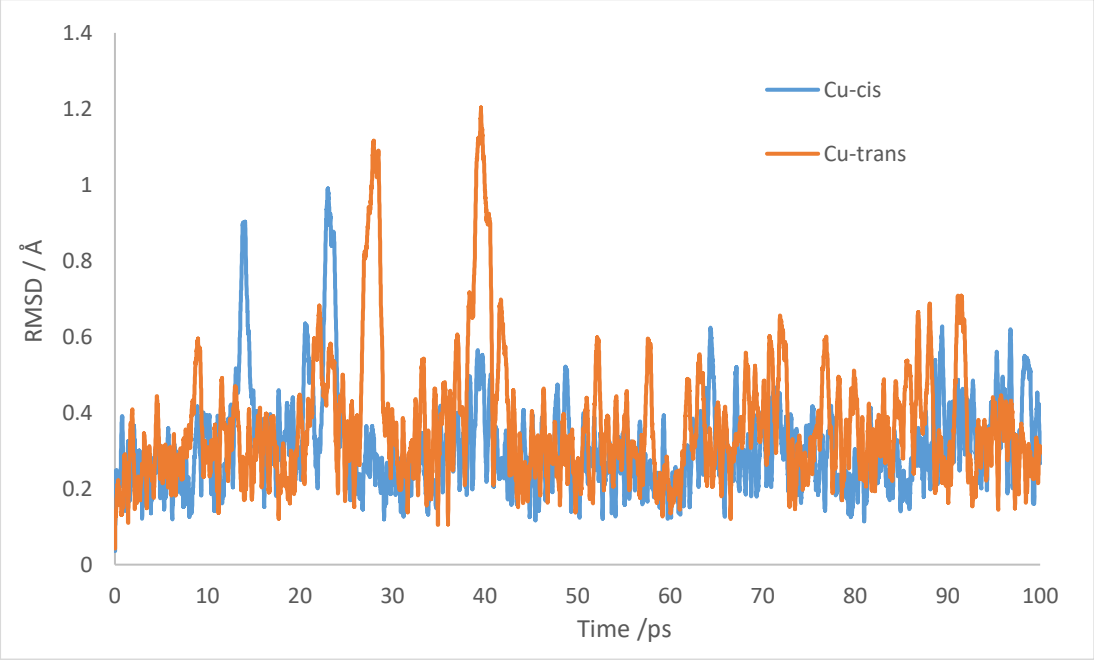

Figure 6: RMSD (Å) over 100 ps MD simulation for cis and trans Cu-GHK

Table 1: RMSD average and standard deviation

	Ave	**SD**	**MIN**	**MAX**
Cu-trans	0.37	0.17	0.04	1.20
Free-trans	0.35	0.10	0.04	0.70
Cu-cis	0.31	0.12	0.04	0.99
Free-cis	0.29	0.09	0.03	0.63

Selected bond distances corresponding to the first coordination sphere of copper, as labelled in Figure 7, were analysed and summarized in Table 2. This showed only small deviations for

most bonds identified: only apical Cu—O coordination from carboxylate of Lys is found to deviate significantly from the starting value, reaching values as large as 3.72 Å, with standard deviation twice as large as found for other bonds. All four equatorial bonds to Cu are more stable, with averages close to 2.0 Å and small standard deviations, although distances as long as 2.6 Å are observed in specific frames. Taken together, this data suggests that copper binding to the peptide remains stable over the timescale of 100 ps.

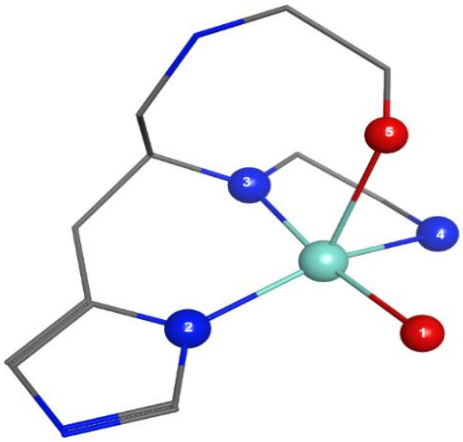

Figure 7: Numbering of Cu-ligand atoms (remaining atoms omitted for clarity)

Table 2: bond distance trajectory analysis (Å)

cis1	**Ave**	**SD**	**MIN**	**MAX**
1 (Cu-OH_2)	2.09	0.10	1.80	2.65
2 (Cu-N_{His})	2.03	0.08	1.80	2.35
3 (Cu-N_{pept})	1.92	0.07	1.71	2.27
4 (Cu-N_{NH2})	2.15	0.10	1.81	2.61
5 (Cu-O_{COO})	2.28	0.21	1.85	3.72

trans1	**Ave**	**SD**	**MIN**	**MAX**
1	2.13	0.12	1.79	2.66
2	2.02	0.07	1.79	2.37
3	1.94	0.07	1.73	2.24
4	2.14	0.10	1.85	2.73
5	2.23	0.18	1.87	3.61

Following the success of the GFN*2*-xTB approach, we explored whether this method could identify the known binding mode of Cu(II) to GHK, using the associated conformer–rotamer ensemble sampling tool (CREST). Initial input consisted of three separated fragments in one file, namely N-deprotonated GHK, Cu and H_2O, with conformational search used for non-covalent mode to prevent dissociation. The most stable conformer generated, shown in Figure 8, is almost identical to *trans* optimized geometry that identified from LFMM conformational search followed by GFN2-XTB (RMSD= 0.335Å). This shows that that GFN2-XTB coupled with the high efficiency of sampling in the CREST approach could be a valuable means for predicting optimal binding mode for metals. However, we note that for this method to succeed it is necessary for the correct protonation state of the peptide to be specified in advance, which may limit application of this approach if this is not known *a priori.*

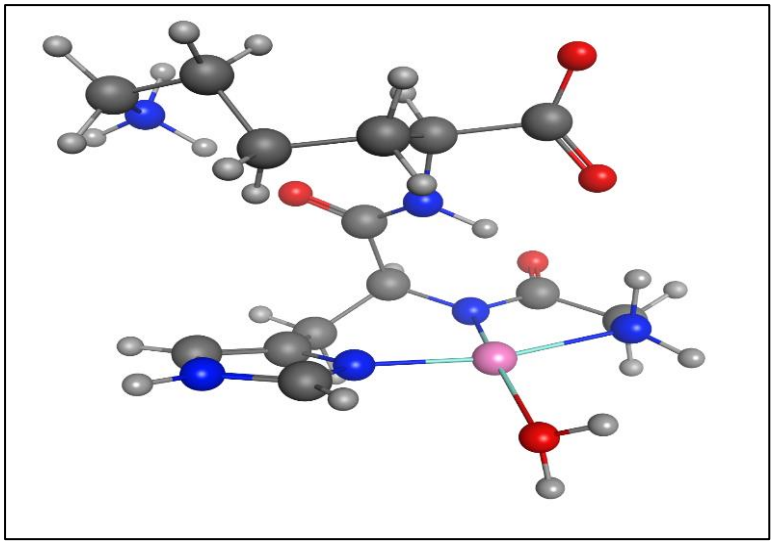

Figure 8: Most stable conformer CREST conformational search

Conclusions

Cu-GHK is used as a model to evaluate the semi-empirical tight binding method performance termed as GFN2-xTB, which can be then applied on larger metal-peptide systems such as amyloid-β. The main purpose of this paper is to study the ability of this approach in predicting the geometry an energy of Cu-GHK conformations. We find that it is able to reproduce the lowest energy conformer and its geometry, as well as the relative energies of higher energy conformers, when compared to DFT data. In addition, the same method coupled with efficient metadynamics sampling tool CREST correctly predicted the binding site of Cu to GHK. The efficiency of the GFN2-xTB method allowed MD simulation of Cu-GHK, indicating that all four equatorial bonds remain stable over 100 ps in two different conformations, while the apical bond to C-terminal carboxylate is more variable.

Acknowledgements

NA is sponsored by government of Saudi Arabia Ministry of Education scholarship. We are grateful to Advanced Research Computing @ Cardiff (ARCCA) and Supercomputing Wales for computing resources.

References

1. Schlesinger, D. H., Pickart, L. & Thaler, M. M. Growth-modulating serum tripeptide is glycyl-histidyl-lysine. *Experientia* **33**, 324–325 (1977).

2. Pickart, L. & Thaler, M. M. Tripeptide in human serum which prolongs survival of normal liver cells and stimulates growth in neoplastic liver. *Nat New Biol* **243**, 85–87 (1973).

3. Rozga, M., Sokolowska, M., Protas, A. M. & Bal, W. Human serum albumin coordinates Cu(II) at its N-terminal binding site with 1 pM affinity. *J Biol Inorg Chem* **12**, 913–918 (2007).

4. Hureau, C. *et al.* X-ray and Solution Structures of CuIIGHK and CuIIDAHK Complexes: Influence on Their Redox Properties. *Chem. – A Eur. J.* **17**, 10151–10160 (2011).

5. Lau, S. J. & Sarkar, B. The interaction of copper(II) and glycyl-l-histidyl-l-lysine, a growth-modulating tripeptide from plasma. *Biochem. J.* **199**, 649–656 (1981).

6. Perkins, C. M. *et al.* The structure of a copper complex of the growth factor glycyl-L-histidyl-L-lysine at 1.1 Å resolution. *Inorganica Chim. Acta* **82**, 93–99 (1984).

7. Freedman, J. H., Pickart, L., Weinstein, B., Mims, W. B. & Peisach, J. Structure of the Glycyl-L-histidyl-L-lysine-Copper(II) Complex in Solution. *Biochemistry* **21**, 4540–4544 (1982).

8. Siméon, A., Emonard, H., Hornebeck, W. & Maquart, F.-X. The tripeptide-copper complex glycyl-L-histidyl-L- lysine-Cu2+ stimulates matrix metalloproteinase-2 expression by fibroblast cultures. *Life Sci.* **67**, 2257–2265 (2000).

9. Ehrlich, H. P. Stimulation of skin healing in immunosuppressed rats. in *Symposium on collagen and skin repair* (1991).

10. McCormack, M. C., Nowak, K. C. & Koch, R. J. The Effect of Copper Tripeptide and Tretinoin on Growth Factor Production in a Serum-Free Fibroblast Model. *JAMA Facial Plast. Surg.* **3**, 28–32 (2001).

11. Pickart, L., Vasquez-Soltero, J. M. & Margolina, A. The Human Tripeptide GHK-Cu in Prevention of Oxidative Stress and Degenerative Conditions of Aging: Implications for Cognitive Health. *Oxid. Med. Cell. Longev.* **2012**, 1–8 (2012).

12. Schirer, A., Khoury, Y. El, Faller, P. & Hellwig, P. Similarities and differences of copper and zinc cations binding to biologically relevant peptides studied by vibrational spectroscopies. *JBIC J. Biol. Inorg. Chem.* **22**, 581–589 (2017).

13. Kremennaya, M. A., Soldatov, M. A., Podkovyrina, Y. S., Dadasheva, I. A. & Soldatov, A. V. X-ray spectroscopy study of the Cu(II)GHK peptide complex. *J. Struct. Chem.* **58**, 1213–1219 (2017).

14. Trapaidze, A., Hureau, C., Bal, W., Winterhalter, M. & Faller, P. Thermodynamic study of Cu2+ binding to the DAHK and GHK peptides by isothermal titration calorimetry (ITC) with the weaker competitor glycine. *JBIC J. Biol. Inorg. Chem.* **17**, 37–47 (2012).

15. Hureau, C. *et al.* X-ray and solution structures of Cu IIGHK and Cu IIDAHK complexes: Influence on their redox properties. *Chem. - A Eur. J.* **17**, 10151–10160 (2011).

16. Guilloreau, L., Combalbert, S., Sournia-Saquet, A., Mazarguil, H. H. & Faller, P. Redox chemistry of copper-amyloid-beta: The generation of hydroxyl radical in the presence of ascorbate is linked to redox-potentials and aggregation state. *CHEMBIOCHEM* **8**, 1317–1325 (2007).

17. Peverati, R. & G. Truhlar, D. M11-L: A Local Density Functional That Provides Improved Accuracy for Electronic Structure Calculations in Chemistry and Physics. *J. Phys. Chem. Lett.* **3**, 117–124 (2011).

18. Dasari, S. & Bernard Tchounwou, P. Cisplatin in cancer therapy: Molecular mechanisms of action. *Eur. J. Pharmacol.* **740**, 364–378 (2014).

19. Hartmann, M. Molecular mechanics. Von ULRICH BURKERT und NORMAN L. ALLINGER. ACS Monograph 177. Washington: American Chemical Society 1982. 430 S., US $ 77.95. *Acta Polym.* **35**, 528 (1984).

20. Atavin, E. G., Mastryukov, V. S., Allinger, N. L., Almenningen, A. & Seip, R. Molecular structure of cyclododecane, C12H24, as determined by electron diffraction and molecular mechanics. *J. Mol. Struct.* **212**, 87–95 (1989).

21. Brooks, B. R. *et al.* CHARMM: A program for macromolecular energy, minimization, and dynamics calculations. *J. Comput. Chem.* **4**, 187–217 (1983).

22. Weiner, P. K. & Kollman, P. A. AMBER: Assisted model building with energy refinement. A general program for modeling molecules and their interactions. *J. Comput. Chem.* **2**, 287–303 (1981).

23. Weiner, S. J., Kollman, P. A., Nguyen, D. T. & Case, D. A. An all atom force field for simulations of proteins and nucleic acids. *J. Comput. Chem.* **7**, 230–252 (1986).

24. Mayo, S. L., Olafson, B. D. & Goddard, W. A. DREIDING: a generic force field for molecular simulations. *J. Phys. Chem.* **94**, 8897–8909 (1990).

25. S. Allured, V., M. Kelly, C. & R. Landis, C. SHAPES empirical force field: new treatment of angular potentials and its application to square-planar transition-metal complexes. *J. Am. Chem. Soc.* **113**, 1–12 (2002).

26. Deeth, R. J. Computational modelling of transition metal centres. in *Coordination Chemistry* 1–42 (Springer Berlin Heidelberg, 1995). doi:10.1007/BFb0036824.

27. Marques, H. M., Egan, T. J. & de Villiers, K. A. Structure and Function: Insights into Bioinorganic Systems from Molecular Mechanics Calculations. in *Structure and Function* (ed. Comba, P.) 87–109 (Springer Netherlands, 2010). doi:10.1007/978-90-481-2888-4_4.

28. Wiesemann, F., Teipel, S., Krebs, B. & Hoeweler, U. Force Field Calculations on the Structures of Transition Metal Complexes. 1. Application to Copper(II) Complexes in Square-Planar Coordination. *Inorg. Chem.* **33**, 1891–1898 (1994).

29. Gkionis, K. & Platts, J. A. QM/MM investigation into binding of square-planar platinum complexes to DNA fragments. *JBIC J. Biol. Inorg. Chem.* **14**, 1165 (2009).

30. Spiegel, K., Rothlisberger, U. & Carloni, P. Cisplatin Binding to DNA Oligomers from Hybrid Car-Parrinello/Molecular Dynamics Simulations. *J. Phys. Chem. B* **108**, 2699–

2707 (2004).

31. Robertazzi, A. & Platts, J. A. A QM/MM Study of Cisplatin–DNA Oligonucleotides: From Simple Models to Realistic Systems. *Chem. – A Eur. J.* **12**, 5747–5756 (2006).

32. Matsui, T., Shigeta, Y. & Hirao, K. Multiple Proton-Transfer Reactions in DNA Base Pairs by Coordination of Pt Complex. *J. Phys. Chem. B* **111**, 1176–1181 (2007).

33. Spiegel, K. & Magistrato, A. Modeling anticancer drug–DNA interactions via mixed QM/MM molecular dynamics simulations. *Org. Biomol. Chem.* **4**, 2507–2517 (2006).

34. Spiegel, K., Rothlisberger, U. & Carloni, P. Duocarmycins Binding to DNA Investigated by Molecular Simulation. *J. Phys. Chem. B* **110**, 3647–3660 (2006).

35. V. Vargiu, A., Ruggerone, P., Magistrato, A. & Carloni, P. Anthramycin−DNA Binding Explored by Molecular Simulations. *J. Phys. Chem. B* **110**, 24687–24695 (2006).

36. Tuttle, T., Kraka, E., Thiel, W. & Cremer, D. A QM/MM Study of the Bergman Reaction of Dynemicin A in the Minor Groove of DNA. *J. Phys. Chem. B* **111**, 8321–8328 (2007).

37. Sundaresan, N., K. S. Pillai, C. & H. Suresh, C. Role of Mg2+ and Ca2+ in DNA Bending: Evidence from an ONIOM-Based QM-MM Study of a DNA Fragment. *J. Phys. Chem. A* **110**, 8826–8831 (2006).

38. J. Burton, V., J. Deeth, R., M. Kemp, C. & J. Gilbert, P. Molecular Mechanics for Coordination Complexes: The Impact of Adding d-Electron Stabilization Energies. *J. Am. Chem. Soc.* **117**, 8407–8415 (2002).

39. Deeth, R. J., Anastasi, A., Diedrich, C. & Randell, K. Molecular modelling for transition metal complexes: Dealing with d-electron effects. *Coord. Chem. Rev.* **253**, 795–816 (2009).

40. Deeth, R. J. & Hearnshaw, L. J. A. Molecular modelling of Jahn–Teller distortions in Cu(ii)N6 complexes: elongations{,} compressions and the pathways in between. *Dalt. Trans.* 1092–1100 (2006) doi:10.1039/B509274D.

41. Deeth, R. J. & Hearnshaw, L. J. A. Molecular modelling for coordination compounds: Cu(ii)–amine complexes. *Dalt. Trans.* 3638–3645 (2005) doi:10.1039/B507295F.

42. Deeth, R. J. A test of ligand field molecular mechanics as an efficient alternative to QM/MM for modelling metalloproteins: the structures of oxidised type I copper centres. *Chem. Commun.* 2551–2553 (2006) doi:10.1039/B604290B.

43. Do, H., J. Deeth, R. & A. Besley, N. Computational Study of the Structure and Electronic Circular Dichroism Spectroscopy of Blue Copper Proteins. *J. Phys. Chem. B* **117**, 8105–8112 (2013).

44. Turner, M., Platts, J. A. & Deeth, R. J. Modeling of Platinum-Aryl Interaction with Amyloid-β Peptide. *J. Chem. Theory Comput.* **12**, 1385–1392 (2016).

45. Turner, M., Mutter, S. T., Deeth, R. J. & Platts, J. A. Ligand field molecular dynamics simulation of Pt(II)-phenanthroline binding to N-terminal fragment of amyloid-beta peptide. *PLoS One* **13**, e0193668 (2018).

46. Mutter, S. T., Turner, M., J. Deeth, R. & A. Platts, J. Metal Binding to Amyloid-β1–42: A Ligand Field Molecular Dynamics Study. *ACS Chem. Neurosci.* **9**, 2795–2806 (2018).

47. Ćendić, M., Matović, Z. D. & Deeth, R. J. Molecular modeling for Cu(II)-aminopolycarboxylate complexes: Structures, conformational energies, and ligand binding affinities. *J. Comput. Chem.* **34**, 2687–2696 (2013).

48. Bentz, A. *et al.* Modeling of the Various Minima on the Potential Energy Surface of Bispidine Copper(II) Complexes: A Further Test for Ligand Field Molecular Mechanics. *Inorg. Chem.* **47**, 9518–9527 (2008).

49. Tai, H. C. *et al.* Combined theoretical and computational study of interstrand DNA guanine-guanine cross-linking by trans -[Pt(pyridine) 2] derived from the photoactivated prodrug trans,trans,trans -[Pt(N 3) 2(OH) 2(pyridine) 2]. *Inorg. Chem.* **51**, 6830–6841 (2012).

50. Grimme, S., Bannwarth, C. & Shushkov, P. A Robust and Accurate Tight-Binding Quantum Chemical Method for Structures, Vibrational Frequencies, and Noncovalent

Interactions of Large Molecular Systems Parametrized for All spd-Block Elements (Z = 1-86). *J. Chem. Theory Comput.* **13**, 1989–2009 (2017).

51. Bannwarth, C., Ehlert, S. & Grimme, S. GFN2-xTB—An Accurate and Broadly Parametrized Self-Consistent Tight-Binding Quantum Chemical Method with Multipole Electrostatics and Density-Dependent Dispersion Contributions. *J. Chem. Theory Comput.* **15**, 1652–1671 (2019).

52. Bursch, M., Neugebauer, H. & Grimme, S. Structure Optimisation of Large Transition-Metal Complexes with Extended Tight-Binding Methods. *Angew. Chemie Int. Ed.* **58**, 11078–11087 (2019).

53. Grimme, S. Exploration of Chemical Compound, Conformer, and Reaction Space with Meta-Dynamics Simulations Based on Tight-Binding Quantum Chemical Calculations. *J. Chem. Theory Comput.* **15**, 2847–2862 (2019).

54. Kovács, A., Cz. Dobrowolski, J., Ostrowski, S. & Rode, J. E. Benchmarking density functionals in conjunction with Grimme's dispersion correction for noble gas dimers (Ne2, Ar2, Kr2, Xe2, Rn2). *Int. J. Quantum Chem.* **117**, e25358 (2017).

55. Bursch, M., Hansen, A. & Grimme, S. Fast and Reasonable Geometry Optimization of Lanthanoid Complexes with an Extended Tight Binding Quantum Chemical Method. *Inorg. Chem.* **56**, 12485–12491 (2017).

56. Labute, P. LowModeMD—Implicit Low-Mode Velocity Filtering Applied to Conformational Search of Macrocycles and Protein Loops. *J. Chem. Inf. Model.* **50**, 792–800 (2010).

57. M. Ferguson, D. & J. Raber, D. A new approach to probing conformational space with molecular mechanics: random incremental pulse search. *J. Am. Chem. Soc.* **111**, 4371–4378 (2002).

58. Cornell, W. D. *et al.* A Second Generation Force Field for the Simulation of Proteins, Nucleic Acids, and Organic Molecules. *J. Am. Chem. Soc.* **117**, 5179–5197 (1995).

59. Mutter, S. T., Deeth, R. J., Turner, M. & Platts, J. A. Benchmarking of copper(II) LFMM parameters for studying amyloid- peptides. *J. Biomol. Struct. Dyn.* **36**, 1145–

1153 (2018).

60. Chemical Computing Group Inc. Molecular Operating Environment (MOE). (2013).

61. Lee, C., Yang, W. & Parr, R. G. Development of the Colle-Salvetti correlation-energy formula into a functional of the electron density. *Phys. Rev. B* **37**, 785–789 (1988).

62. Grimme, S. Semiempirical GGA-type density functional constructed with a long-range dispersion correction. *J. Comput. Chem.* **27**, 1787–1799 (2006).

63. Schäfer, A., Horn, H. & Ahlrichs, R. Fully optimized contracted Gaussian basis sets for atoms Li to Kr. *J. Chem. Phys.* **97**, 2571–2577 (1992).

64. Weigend, F. & Ahlrichs, R. Balanced basis sets of split valence{,} triple zeta valence and quadruple zeta valence quality for H to Rn: Design and assessment of accuracy. *Phys. Chem. Chem. Phys.* **7**, 3297–3305 (2005).

65. Perdew, J. P., Burke, K. & Ernzerhof, M. Generalized Gradient Approximation Made Simple. *Phys. Rev. Lett.* **77**, 3865–3868 (1996).

66. Perdew, J. P., Burke, K. & Ernzerhof, M. Generalized Gradient Approximation Made Simple [Phys. Rev. Lett. 77, 3865 (1996)]. *Phys. Rev. Lett.* **78**, 1396–1396 (1997).

67. Perdew, J. P., Ernzerhof, M. & Burke, K. Rationale for mixing exact exchange with density functional approximations. *J. Chem. Phys.* **105**, 9982–9985 (1996).

68. Adamo, C. & Barone, V. Toward reliable density functional methods without adjustable parameters: The PBE0 model. \j*cp* **110**, 6158–6170 (1999).

69. Grimme, S., Antony, J., Ehrlich, S. & Krieg, H. A consistent and accurate ab initio parametrization of density functional dispersion correction (DFT-D) for the 94 elements H-Pu. *J. Chem. Phys.* **132**, 154104 (2010).

70. Zhao, Y. & Truhlar, D. G. A new local density functional for main-group thermochemistry, transition metal bonding, thermochemical kinetics, and noncovalent interactions. *J. Chem. Phys.* **125**, 194101 (2006).

71. Chai, J.-D. & Head-Gordon, M. Long-range corrected hybrid density functionals with damped atom–atom dispersion corrections. *Phys. Chem. Chem. Phys.* **10**, 6615–6620

(2008).

72. FRISCH & J., M. GAUSSIAN09. *http://www.gaussian.com/*.

73. Neese, F. The ORCA program system. *Wiley Interdiscip. Rev. Comput. Mol. Sci.* **2**, 73–78 (2012).

74. Bannwarth, C., Ehlert, S. & Grimme, S. GFN2-xTB - An Accurate and Broadly Parametrized Self-Consistent Tight-Binding Quantum Chemical Method with Multipole Electrostatics and Density-Dependent Dispersion Contributions. *J. Chem. Theory Comput.* **15**, 1652–1671 (2019).

75. Humphrey, W., Dalke, A. & Schulten, K. VMD: Visual molecular dynamics. *J. Mol. Graph.* **14**, 33–38 (1996).

76. Pracht, P., Grimme, S. CREST.

77. Grimme, S. *et al.* Fully Automated Quantum-Chemistry-Based Computation of Spin–Spin-Coupled Nuclear Magnetic Resonance Spectra. *Angew. Chemie Int. Ed.* **56**, 14763–14769 (2017).